Nanosize Polyacrylamide/SiO$_2$ Composites by Inverse Microemulsion Polymerization

Pallavi Bhardwaj[a]; Sujata Singh[a]; Vaishali Singh[a]; Saroj Aggarwal[a]; U. K. Mandal[b]
[a] University School of Basic and Applied Science, GGS Indraprastha University, Delhi, India [b] University School of Chemical Technology, GGS Indraprastha University, Delhi, India

PLEASE SCROLL DOWN FOR ARTICLE

Taylor & Francis
Taylor & Francis Group

Nanosize Polyacrylamide/SiO$_2$ Composites by Inverse Microemulsion Polymerization

Pallavi Bhardwaj
Sujata Singh
Vaishali Singh
Saroj Aggarwal
University School of Basic and Applied Science, GGS Indraprastha University, Delhi, India

U. K. Mandal
University School of Chemical Technology, GGS Indraprastha University, Delhi, India

Nanosize polyacrylamide/silica (PAM/SiO$_2$) composites were prepared by water-in-oil (W/O) microemulsion process. In this system, aqueous solution of acrylamide containing disperse 10 nm size silicon dioxide was used as the dispersed phase of the microemulsion while the dispersion medium was sodium bis (2-ethylhexyl) sulfosuccinate (AOT)/toluene solution. The size of the synthesized PAM/SiO$_2$ nanocomposites was 38–76 nm as determined by dynamic light scattering (DLS). The incorporation of nanosize silica filler reduces the particle size of PAM latex. It had also been found that the size of composite particles decreases with increasing filler loading along with better polydispersity. The presence of silica particles in the polymer latex particles and interaction of polymer chains with silica particles in hybrid nanocomposites were characterized by Fourier transform infra red spectrophotometry (FTIR), thermogravimetry analysis (TGA) and differential scanning calorimetry (DSC). The TGA results showed improved thermoresistance and high thermal stability behavior of hybrid composites. The DSC measurements revealed that the incorporation of filler favors crystallization, increases the enthalpy of melting and thermal stabilization of the synthesized composite particles. A scanning electron microscope (SEM) was used to study the morphology and topography of the prepared nanocomposites.

404

INTRODUCTION

Nanocomposites are a relatively new class of materials with ultrafine phase dimensions, typically of the order of a few nanometers [1–4]. Organic/inorganic hybrids offer the possibility of a new generation of nanostructured materials with diverse applications such as catalysts, [5] electronic or photonic devices, [6] and sensors for volatile organic compounds [7]. Furthermore, the incorporation of inorganic materials on the nanoscale can enhance the fire retardancy [8] and mechanical strength [9] of organic polymers and coatings.

Microemulsions have received considerable interest because of their small droplet size and complex structural behavior. The structural features depending on the microemulsion composition can be used to prepare nanosize composite particles through in-situ polymerization in the presence of dispersed inorganic nanoparticles, which become trapped or encapsulated in the matrix after polymerization [10–12]. The adjustable size of the micelles is a valuable tool for tailoring the dispersion of inorganic particles as well as control of the composite particle size. In order to avoid agglomeration of fillers, nanocomposites were synthesized by in-situ polymerization. In-situ polymerization is a method where at first inorganic fillers or reinforcements are dispersed in the monomer or monomer solution, and then this mixture is polymerized using the usual polymerization techniques. The most commonly used nanoparticles are silica (SiO_2), titanium dioxide (TiO_2), carbon black, aluminium oxide (Al_2O_3), zinc oxide (ZnO), and calcium carbonate ($CaCO_3$) [13–15].

In this field, silica is the most commonly used inorganic support for two main reasons. First, synthesis of monodispersed silica particles is quite easy to perform and well-documented in the literature [16]. Second, various potential applications of silica-based systems are involved: gasliquid chromatography, paintings, catalyst supports, etc. [17]. Owing to the many uses of silica [18–20], different methods for the synthesis of polymer-silica particles have been reported. In those related works, vinyl polymer-silica nanocomposite particles were synthesized [21–23]. Chen et al. reported the synthesis of raspberry-like $PMMA/SiO_2$ nanocomposite particles via a free-radical copolymerization of methyl methacrylate (MMA) with 1-vinylimidazole in the presence of ultrafine aqueous silica sols [24–25]. Most of these reports were related to the nonpolar polymer/silica hybrid materials. As we know, the compatibility between inorganic particles and polymer is not good in these materials, which further restricts the application of hybrid materials.

To our best knowledge, only a few works have reported on the synthesis of nanosize composite particles based on polar polymers through in-situ polymerization methods and the interaction of polar polymer chains with silica particles. The present article describes the synthesis
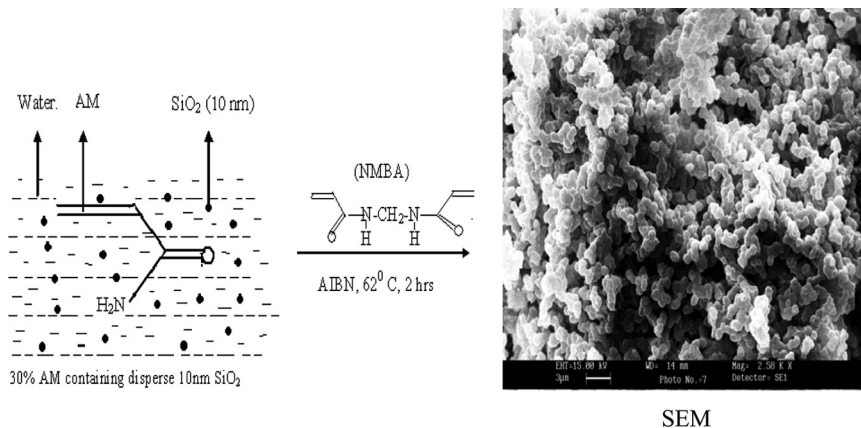
FIGURE 1 Reaction scheme for the formation of polyacrylamide-SiO$_2$ nano-composite by in-situ microemulsion polymerization at 62°C.

of PAM-SiO$_2$ nanocomposites by in-situ W/O microemulsion process (Figure 1), in which water/toluene inverse emulsion was used to make the product become a fine powder. The prepared nanosize nanocomposite particles were characterized by dynamic light scattering (DLS), Fourier transform infrared spectrophotometry (FTIR), differential scanning calorimetry (DSC), thermogravimetry analyzer (TGA), and scanning electron microscopy (SEM).

EXPERIMENTAL

Materials

Acrylamide (AM), 10 nm silicon dioxide (SiO$_2$) and Sodium bis (2-ethyl-hexyl) sulfosuccinate (AOT) were purchased from Aldrich and used directly without further purification. 2,2-Azobisisobutyronitrile (AIBN), purchased from Spectrochem Private Ltd. (India), and extra-pure N,N′-Methylenebisacrylamide (NMBA), from SRL (India), were used as initiator and crosslinker, respectively. Both AIBN and NMBA were used as received. AR grade toluene, received from SRL (India), was distilled prior to use. Double-distilled water drawn from a Millipore purification system was used.

Synthesis of PAM/SiO$_2$ Nanocomposite by W/O Microemulsion

Dispersed silica solution was prepared by adding the desired amount of silica (silicon dioxide) to 13.72 ml of 30% acrylamide aqueous

TABLE 1 The Composition of W/O Microemulsion System for PAM/SiO$_2$ Nanocomposite Synthesis

↓Composition (gm)	AS$_0$	AS$_2$	AS$_5$	AS$_{10}$
Toluene	64.3	64.3	64.3	64.3
AOT	17.86	17.86	17.86	17.86
Water	13.72	13.72	13.72	13.72
AM	4.12	4.12	4.12	4.12
SiO$_2$	0.00	0.103	0.206	0.412
AIBN	0.0412	0.0412	0.0412	0.0412
NMBA	0.0412	0.0412	0.0412	0.0412

solution (Table 1). This suspension was stirred by a magnetic stirrer at 1000 rpm in a 100 ml single-neck round-bottom flask for 2 h for proper dispersion of the silicon dioxide in the aqueous monomer solution. In W/O microemulsion process, 17.86 gm AOT were dissolved in 64.30 gm toluene in a 250 ml conical flask. Now, the above prepared aqueous acrylamide solution containing dispersed SiO$_2$ was added dropwise to the AOT solution to form a W/O microemulsion. This microemulsion was transferred to a 250 ml, 2-neck round-bottom flask fitted with a condenser and a nitrogen gas inlet. It was stirred by magnetic stirrer at 1000 rpm for 6 h. AIBN and NMBA (each 1 wt% of monomer) were added to initiate the polymerization and for crosslinking. The microemulsion was then purged with nitrogen gas for 30 min. The polymerization mixture was heated in a water bath at 62°C under stirring conditions at 400–500 rpm for 2 h. After polymerization, the mixture was cooled to room temperature and acetone was added to precipitate the polymerized product. The precipitates were separated and washed several times through centrifugation first with CH$_3$OH to remove residual monomer and then with toluene to remove AOT. The precipitates were then dried in a vacuum oven at 50°C until constant weight was obtained.

Conventional polyacrylamide was also prepared by W/O microemulsion process without silicon dioxide to compare it with PAM-SiO$_2$ nanocomposites.

CHARACTERIZATION

Dynamic Light Scattering (DLS)

A Malvern Zetasizer Nano Series (Malvern Instruments Limited, U. K.) was used to measure the size of the reverse micelle of

microemulsion droplet, PAM-SiO$_2$ nanocomposites and conventional PAM. The Zetasizer Nano S measures the scattering information close to 180° (backscatter detection) and uses patented NIBS[TM] technology to increase detection sensitivity and reduction in multiple scattering (minimum at 180° hence higher concentration can be measured). The effect of dust particles is greatly reduced.

DLS measurements were performed at 25°C in a square glass cuvette with a round aperture at a fixed angle of 90°. The values of dispersant refractive index and viscosity of toluene were taken to be 1.491 and 0.5500 cP, respectively.

Fourier Transform Infrared Spectroscopy (FTIR)

The FTIR spectra were collected on a SHIMADZU Japan FTIR-8700 Fourier Transform Infrared Spectrophotometer. Samples of isolated particles of prepared nanoparticles were mixed with KBr, homogenized and converted into pellets under a pressure of 8 ton and the absorbance spectra were taken and interpreted.

Thermal Analysis

(a) Thermogravimetric Analysis (TGA)—The TGA analysis was performed using a Perkin-Elmer TGA7 Thermobalance. 3.94 mg of the dried sample in a nitrogen atmosphere were subjected to TGA analysis in the temperature range of 50 to 780°C at scanning rate of 20°C/min.

(b) Differential Scanning Calorimetry (DSC)—Differential scanning calorimetry (DSC Q10, TA Instruments, USA) was used to determine the glass transition temperature of PAM-SiO$_2$ nanocomposites and conventional PAM. About 2–2.5 mg of the sample were sealed in an aluminium DSC pan and heated from 50 to 350°C at a heating rate of 10°C/min under nitrogen purge flow (50 ml/min).

Scanning Electron Microscope (SEM)

The surface morphology of the dried PAM-SiO$_2$ nanocomposites was studied by using scanning electron microscope (LEO 435VP) operated at 15 Kv. Coating was carried out under reduced pressure in an inert argon gas atmosphere (Agar Sputter Coater P7340).

RESULTS AND DISCUSSION

Size Analysis

Dynamic light scattering size analysis has shown that the hydrodynamic diameter (D_H) values of PAM-SiO$_2$ nanocomposites and conventional

TABLE 2 Particle Size of Conventional PAM and PAM-SiO$_2$ Nanocomposites

Samples	D$_H$(nm)	PDI
AS$_0$	76	0.248
AS$_2$	50	0.243
AS$_5$	44	0.171
AS$_{10}$	38	0.389

PAM were in the range of 38–76 nm, depending on the amount of filler content in the prepared nanocomposites. Table 2 summarizes the sizes of conventional PAM and PAM-SiO$_2$ nanocomposites. It is evident that the presence of silicon dioxide (10 nm) in the PAM-SiO$_2$ nanocomposites showed a marked effect on the size of nanocomposites as compared to their conventional PAM. By increasing the amount of silicon dioxide from 2.5 to 10% of monomer in the dispersion medium, a decrease in the particle size was observed. Decrease in particle size of PAM-SiO$_2$ nanocomposites was attributed to homogenous dispersion of silicon dioxide in surfactant solution in such a manner that SiO$_2$ was spread to the fullest both in and around the polyacrylamide [26]. The prepared PAM-SiO$_2$ nanocomposites were monomodal and monodisperse in nature. The width parameter known as polydispersity or polydispersity index (PDI) also shows a declining trend up until the third sample. However, for the fourth sample it is high, i.e. 0.389. The increase in PDI for the fourth sample was probably due to agglomeration of highly charged silicon dioxide nanoparticles due to high loading of the filler.

FTIR Analysis

The FTIR spectra of the dried pure PAM and PAM-SiO$_2$ nanocomposites in absorbance mode are shown in Figure 2. The spectra confirmed that the product contained polyacrylamide and excluded the presence of monomer [27–28]. We found that the FTIR spectra of the prepared nanocomposites and pure PAM are similar, although the spectrum of each nanocomposite shows some changes accompanying the different filler content in the composite. The N-H asymmetric stretching of NH$_2$ was observed in the region 3353–3362 cm^{-1} and N-H symmetric stretching of NH$_2$ from 3198–3200 cm^{-1}. The strong absorption in the region 1652–1663 cm^{-1} can be attributed to the C=O stretching of CO, amide I band and is the most representative type of vibration localized in an individual bond. However, strong peak from 1616 cm^{-1} corresponds to N−H bending of NH$_2$ (δ) and amide II band.
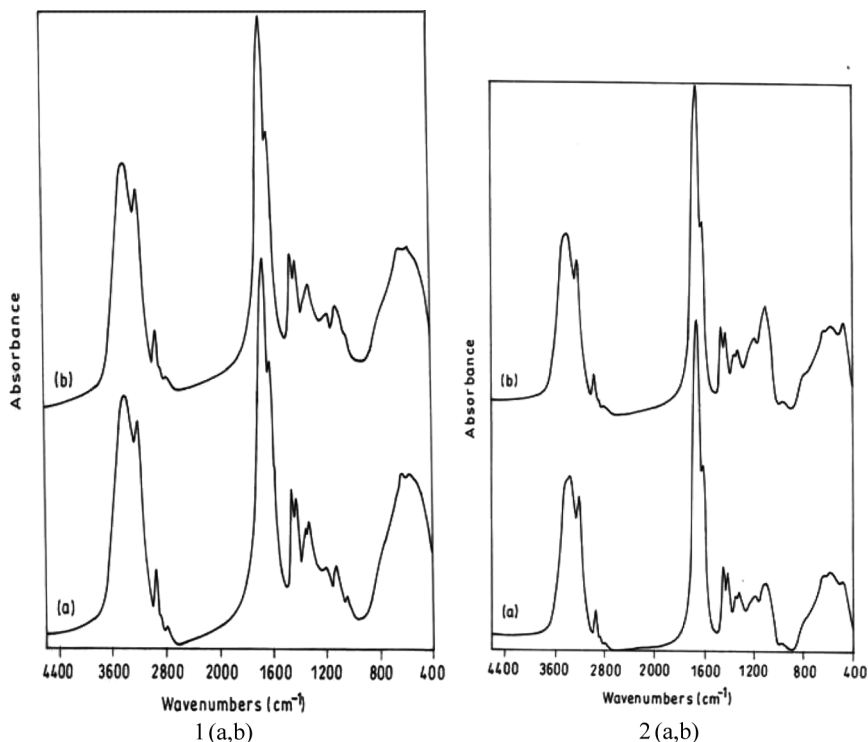
FIGURE 2 The FTIR spectra (range 4400–400 cm^{-1}) of 1(a,b) AS$_0$, AS$_2$ and 2(a,b) AS$_5$, AS$_{10}$.

The peak in the range 1042–1098 cm^{-1} corresponds to Si−O−Si asymmetric bond stretching vibration [29]. The combined NH$_2$ rocking (r) in plane and C−C skeletal vibration also give a weak peak in the region 1125 cm^{-1}. Therefore it could be speculated that the peak at 1125 cm^{-1} is covered by the stronger Si−O stretching vibration in the spectra of composite materials. Table 3 gives the main characteristic peaks assignment of the FTIR spectra. The spectra results clearly indicate the incorporation of nanosize silica particles in the polymeric matrix. At a low dose (AS$_2$) of silica filler the characteristic Si−O stretching (ν) peak at 1098 cm^{-1} disappears but the broadening of the peak at 1225 cm^{-1} indicates the presence of silica filler in polymer particles. Also, with increasing filler loading this characteristic peak appears with enhance intensity. With increasing filler loading, it may be considered that the increase in free silica particles (especially at high dose, AS$_{10}$) attached to polymeric particles may enhance the characteristic strong Si−O stretching (ν) peak at 1098 cm^{-1}.

TABLE 3 Peak Assignment of PAM and the Si-O Stretching According to the Spectrum Shown in the Figure

Peak position (cm^{-1})	Assignment
3353–3362	N−H asym stretching of NH$_2$ (ν)
3198–3200	N−H sym stretching of NH$_2$ (ν)
1652–1663	C=O stretching of CO, amide I band
1616	N−H bending of NH$_2$ (δ), amide II band
1125	C−C skeletal vibration
1042–1098	Si−O−Si asym stretching

In view of the polyacrylamide chain and silica surface interaction, hydrogen bonds should form between the amino groups in the polymer molecules and Si-O linkages. The free Si−O stretching vibration brings out the peak at $1090 \, \text{cm}^{-1}$ and the hydrogen-bonded Si−O stretching vibration with H−bonding shifted to a broad band around $1098 \, \text{cm}^{-1}$. Also in comparison, the FTIR spectra of pure PAM and PAM-composite particles, it is found that the peak intensity ratios of the C=O stretching vibration at $1661 \, \text{cm}^{-1}$ to the N−H bending vibration at $1616 \, \text{cm}^{-1}$ are different as 1.36, 1.43, 1.64, 1.70, corresponding to the increased silica filler in the composite particles. It is believed that the ratio difference comes from the orientation of the carbonyl groups when there is strong hydrogen bonding between the NH$_2$ groups and the SiO$_2$ surface [28].

Thermogravimetric Analysis

The TGA curves of pure polyacrylamide and the prepared nanocomposites with different filler content are shown in Figure 3. The TGA curves of PAM and PAM-SiO$_2$ nanocomposites showed four stages of mass loss with temperature. The first stage as weight loss below 220°C for pure PAM is probably due to absorbed water from the environment and other volatile impurities [30]. For the prepared nanocomposites, the weight loss is about 9–12%. Vilcu et al. [31] studied polyacrylamide samples via thermogravimetric analysis (TGA) and observed an 11% weight loss up to 200°C. They attributed this weight loss to the release of both surface and matrix-bound water from the polymer.

The second weight loss from 260°C to 340°C is about 13–15%. Thermal degradation occurs in this temperature range causing irreversible chemical changes [32]. Here both intra and inter-molecular imidization reactions occur via the pendant amide groups and H$_2$O, NH$_3$
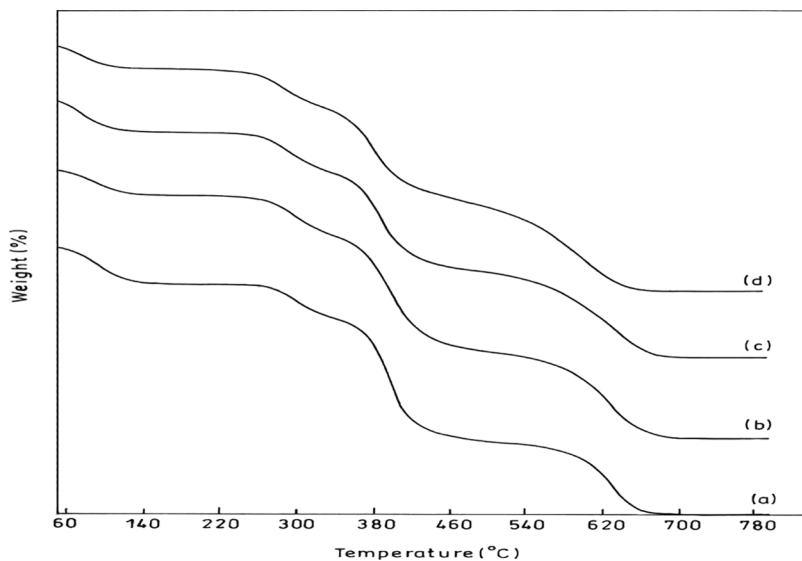
FIGURE 3 TG curves for the samples heated to 780°C. (a) AS_0, (b)AS_2, (c) AS_5, and (d) AS_{10}.

and CO_2 are released as byproducts of the imide formation and degradation [33–34]. It may also be due to some breakdown of the cyclic imides groups at this stage. The third weight loss from 340°C to 500°C is about 47, 44, 37, and 34% for pure polyacrylamide and PAM-SiO$_2$ nanocomposites with different amount of silica. The weight loss which occurs may be due to the decomposition of imides to form nitriles and the release of volatiles such as CO_2 and H_2O, or due to the formation of various substituted glutardimide. This region of weight loss considerably decreases on increasing the amount of silica, which indicates that the presence of silica in the nanocomposites inhibits the formation of nitriles or substituted glutardimide. Also, the decomposition temperature of the composite is higher than the pure polyacrylamide, indicating relatively high thermal stability because of filler-polymer chain interaction. The higher the filler dose the higher thermoresistance is attained for the prepared nanocomposites. The last stage of decomposition occurs at 500 to 700°C with a corresponding weight loss of 26, 30, 31 and 34%. This high temperature decomposition may be due to random bond scission of the polymeric main chain and char formation [35]. Overall, the nanocomposites showed a delayed decomposition compared to the polymeric sample, even though the delayed decomposition is much less significant compared to conventional polymer-filler

composites prepared by melt intercalation. In the present process, the prepared composite particles may act as individual particles coated with a polymer layer, whereas in melt intercalation we have a random distribution of particles inside a three dimensional polymer matrix. The random distribution of silica and filler-polymer interaction hinders the diffusion of the volatile decomposition materials, which contributes to the increased thermal stability [36]. The TG measurement also revealed that the residue left after degradation increases with increasing silica content. The calculated silica contents in the char are 1, 3.5 and 8.5%, corresponding to loading of 2.5, 5 and 10%.

DSC Analysis

Figure 4 shows the heating DSC curves obtained for polyacrylamide-silica composites with different quantities of nanosize silica filler. From these thermograms, the glass-transition temperature (Tg), the melting point temperature (Tm) for which the melting of the crystalline phase occurs; and the melting enthalpy (ΔHm) have been determined. The measured Tg and the two other peaks of the nanocomposites and conventional PAM sample are supported by the results reported in literatures [37–38]. The transition temperature (Tg) and heat flow corresponding to the melting zone were reported in Table 4. The first peak occurs in the range of 97°C to 105°C and is due to the loss of water content in the materials. The second peak is at 266°C and is related to the fusion of the crystalline phase [39]. The small increase of Tg with increasing loading of silica filler may be due to polymer chain filler interaction, or can be ascribed to the gradual immobilization of chain segments in the amorphous parts of the gel. The results also show that ΔHm increases gradually with an increase in the filler content. It reflects the increase of the crystalline zone in the structure of gel.

SEM Analysis

A scanning electron microscope (SEM) reveals the morphologies of the prepared nanocomposites. SEM analysis provides clear morphological information in the dry state. Figure 5 shows SEM images of PAM-SiO₂ nanocomposites with 2.5, 5, and 10% silica fillers and conventional polyacrylamide. As seen in the figure, both polyacrylamide and PAM-SiO₂ nanocomposites are spherical in shape and show a narrow size distribution. Through SEM investigation, it was also observed that the surface morphologies of polyacrylamide and PAM-SiO₂ nanocomposites show slight differences. Polyacrylamide has a smooth surface while the PAM-SiO₂ nanocomposites have a rough surface.
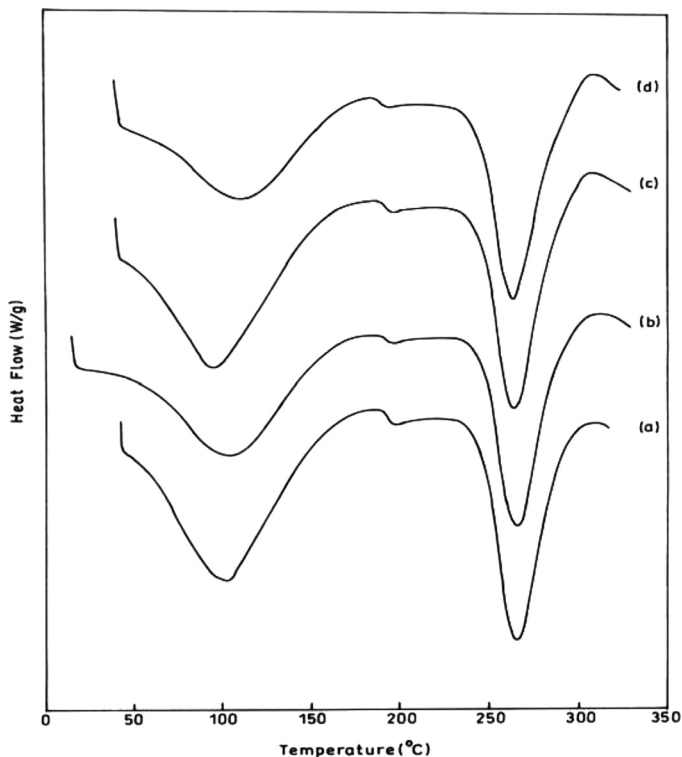
FIGURE 4 DSC curves for the samples heated to 350°C. (a) AS$_0$, (b) AS$_2$, (c) AS$_5$, and (d) AS$_{10}$.

From these micrographs, we can see that the surface of polyacrylamide is very loose while the nanocomposites were compact. It is clear from these micrographs that by increasing the concentration of silica filler from 0 to 2.5%, 5 and 10%, the final nanocomposite particle size was reduced, which supports the DLS results (Table 2).

TABLE 4 Thermal Parameters Obtained by DSC

Sample	Tg (°C)	Tm (°C)	ΔHm (J/g)
AS$_0$	191.95	265.93	228.7
AS$_2$	192.16	266.08	243.0
AS$_5$	193.56	265.40	273.2
AS$_{10}$	193.67	265.18	289.8
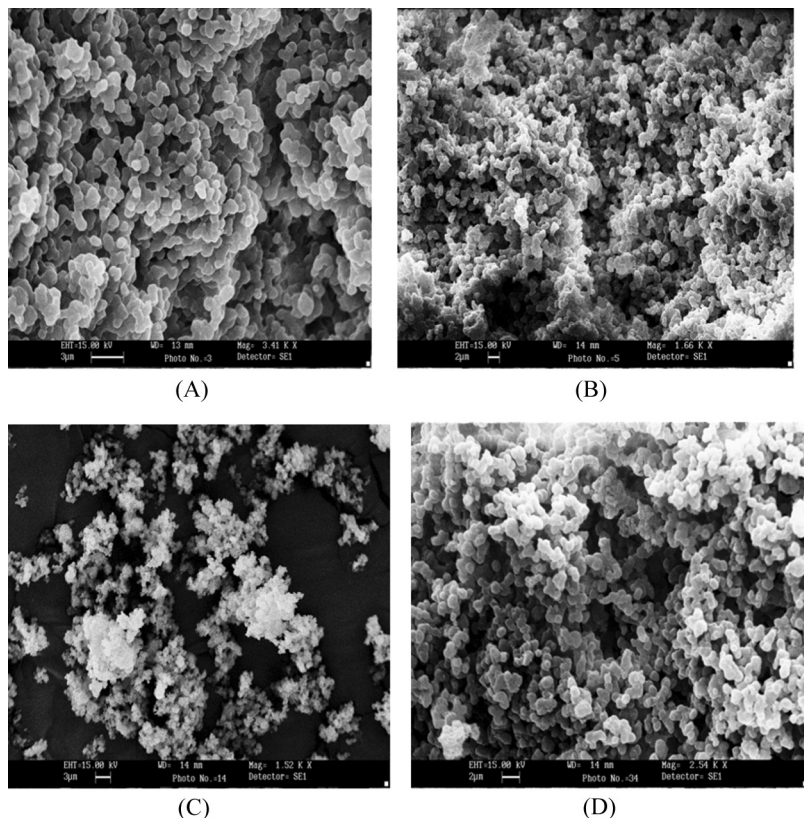
FIGURE 5 SEM micrographs for PAM-SiO$_2$ nanocomposites. (A) AS$_0$, (B) AS$_2$, (C) AS$_5$, and (D) AS$_{10}$.

CONCLUSIONS

Nanosize polyacrylamide/SiO$_2$ composite particles were successfully prepared by the in-situ microemulsion polymerization. Incorporation of nanosize silica filler reduces the particle size of polymer composite with increasing SiO$_2$ loading. The FTIR results show the strong interaction of the polymer chain with silica filler through hydrogen bonding of NH$_2$ group and oxygen of Si$-$O linkage. The Tg and % crystallinity of the nanocomposites increased with increasing amounts of the SiO$_2$ nanoparticles.

REFERENCES

[1] Pomogailo, D., *Russian Chem Rev*. **69**, 53 (2000).
[2] Kickelbick, G. and Schubert, U., *Monatsh. Chem*. **132**, 13 (2001).

[3] Schubert, U., *Chem. Mater.* **13**, 3487 (2001).

[4] Loy, A., *Mater. Bull.* **26**, 364 (2001).

[5] Bugnon, P., *Progr. Org. Coat.* **29**, 39 (1996).

[6] Zhu, J., Morgan, A. B., Lamelas, F.J., and Wilkie, C., *Chem Mater.* **13**, 3774 (2001).

[7] Chigwada, G. and Wilkie, C., *Polym. Degrad. Stab.* **81**, 551 (2003).

[8] Hsiao, K. T., Alms, J., and Advani, S. G., *Nanotechnology* **14**, 791 (2003).

[9] Pu, Z. C., Mark, J. E., Jethmalani, J. M., and Ford, W. T., *Chem. Mater.* **9**, 2442 (1997).

[10] Wang, Q., Xia, H. S., and Zhang, C. H., *J. Appl. Poly. Sci.* **80**, 478 (2001).

[11] Yang, Y. H. and Dan, Y., *Colloid. Polym. Sci.* **281**, 794 (2003).

[12] Jiang, L. and Dan, Y., *Colloid. Polym. Sci.* **282**, 1374 (2004).

[13] Haga, Y., Watanabe, T., and Yosomiya, Y., *Die Angew Makromol. Chem.* **189**, 23 (1991).

[14] Yu, J., Guo, Z. X., and Gao, Y. F., *Macromol. Rapid Commun.* **22**, 1261 (2001).

[15] Bechthold, N., Tiarks, F., Willert, M., Landfester, K., and Antonietti, M., *Macromol. Symp.* **151**, 549 (2000).

[16] Stober, W., Fink, A., and Bohn, E., *J. Colloid Interface Sci.* **26**, 62 (1968).

[17] Xia, Y. N., Gates, B., and Yin, Y. D., *Adv. Mater.* **12**, 693 (2000).

[18] Godovsky, D. Yu., Varfolomeev, A. E., Zaretsky, D. F., Chandrakanthi, R. L. N., Kundig, A., Weder, C., and Caseri, W., *J. Mater. Chem.* **11**, 2465 (2001).

[19] Gill, M., Mykytiuk, J., Armes, S. P., Edwards, J. L., Yeates, T., Moreland, P. J., and Mollett, C., *Chem. Commun.* **108**, (1992).

[20] Maeda, S. and Armes, S. P., *J. Colloid Interface Sci.* **159**, 257 (1993).

[21] Percy, M. J., Amalvy, J. I., Randall, D. P., Armes, S. P., Greaves, S. J., and Watts, J. F., *Langmuir* **20**, 2184 (2004).

[22] Percy, M. J., Michailidou, V., and Armes, S. P., *Langmuir* **19**, 2072 (2003).

[23] Percy, M. J., Barthet, C., Lobb, J. C., Khan, M. A., Lascelles, S. F., Vamvakaki, M., and Armes, S. P., *Langmuir* **16**, 6913 (2000).

[24] Chen, M., Wu, L. M., Zhou, S. X., and You, B., *Macromolecules*, **37**, 9613 (2004).

[25] Chen, M., Zhou, S. X., You, B., and Wu, L. M., *Macromolecules* **38**, 6411 (2005).

[26] Voorn, D. J., Ming, W., and Herk, van A. M., *Macromolecules* **39**, 2137 (2006).

[27] Yan, F., Zheng, C., Zhai, X., and Zhao, D., *J. Appl. Polym. Sci.* **67**, 747 (1998).

[28] Lu, X. and Mi, Yongli, *Macromolecules* **38**, 839 (2005).

[29] Jang, J. and Park, H., *J. Appl. Polym. Sci.* **83**, 1817 (2002).

[30] Silva, M., Dutra, E. R., Mano, V., and Machado, J. C., *Polym. Degrad. Stab.* **67**, 491 (2000).

[31] Vilcu, R., Irinei, F., Ionescu-Bujor, J., Olteanu, M., and Demetrescu, I., *J. Therm. Anal.* **30**, 495 (1985).

[32] Van Dyke, J. D. and Kasperski, K. L., *J. Polym. Sci., Part A: Polym. Chem.* **31** (7), 1807 (1993).

[33] Leung, W. M., Axelson, D. E., and Van Dyke, J. D, *J. Polym. Sci. Part A: Polym. Chem.* **25** (7), 1825 (1987).

[34] Toth, I., Szepvolgyi, J., Jakab, E., Szabo, P., and Szekely, T., *Thermochim. Acta* **170**, 155 (1990).

[35] Vilcu, R., Irinei, F., Ionescu-Bujor, J., Olteanu, M., and Demetrescu, I., *J. Appl. Polym. Sci.* **33**, 2431 (1985).

[36] Burnside, S. D. and Giannelis, E. P., *Chem. Mater.* **7**, 1597 (1995).

[37] Sairam, M., Babu, V. R., Naidu, B. V. K., and Aminabhavi, T. M., *Int. J. Pharmaceutics* **320**, 131 (2006).

[38] Janigova, I., Csomorova, K., Stillhammerova, M., and Barton, J., *Macromol. Chem. Phys.* **195**, 3609 (1994).

[39] Ferreira, L. and Vidal, M. M., *Chem.Educator* **6**, 100 (2001).